BROADBAND MAXIMUM LIKELIHOOD ESTIMATION OF SHALLOW OCEAN PARAMETERS USING SHIPPING NOISE

Christoph F. Mecklenbräuker

Siemens AG, PSE TN MNR
A–1101 Vienna/Austria, cfm@ieee.org

Alex Gershman

Dept. ECE, McMaster Univ., Hamilton
L8S 4K1 Ontario, gershman@ieee.org

ABSTRACT

In this paper, environmental parameter estimation for a shallow ocean is addressed by using wideband shipping noise as a source of acoustic energy. Unknown locations of the broadband acoustic sources are estimated simultaneously with the ocean depth using the approximate Conditional Maximum Likelihood Estimator (CMLE). This procedure is tested via computer simulations and applied to the experimental hydrophone towed array data.

1. INTRODUCTION

Cost-efficient estimation of the geophysical structure of marine sediments just beneath the seafloor is an important topic of research in monitoring of coastal areas. Model-based methods that attempt to invert the acoustic field for obtaining a detailed and global estimate of the seafloor structure have been widely investigated in the past few years [1]. These methods require relatively sophisticated and costly acoustic sensing devices. Regarding the experimental aspect, most studies reported so far required data measurement setups involving extremely long arrays and sound sources either towed or suspended from auxiliary ships. In an effort carried out under MAST II, it was shown that geoacoustic parameter estimation is also possible using a moderate aperture horizontal linear array allowing for the use of a *single* ship towing both the source and the receiver [2].

Recently, some results have been obtained for simultaneous estimation of environmental parameters, source location and receiver calibration [1]. It is shown in [1] that bottom parameter estimation as an optimization procedure for a goal-function allows direct inclusion of the source location parameters into the search space. In practice, this increases the computational burden of the estimation procedure.

From the numerical point of view, estimation of environmental parameters is a highly non-linear and non-convex optimization problem in a high-dimensional bounded domain. These inverse problems are ill-posed, so some sort of regularization scheme is necessary, cf. [5, 6]. Various cost-functions have been proposed in the literature, most of them for the single-source / single-frequency case. The single-frequency case is particularly badly behaved in terms of ambiguity, which can be partly overcome in a fully broadband treatment.

The aim of this paper is to demonstrate experimentally that the broadband CMLE combined with a simplistic ocean waveguide model allows to estimate source and environmental parameters simultaneously with a good accuracy.

supported in part by the Natural Sciences and Engineering Research Council (NSERC) of Canada.

2. PROPAGATION MODEL

The Green's Function $G(\underline{r}, \underline{r}_\circ, \omega)$ is the acoustic response at location $\underline{r} = (r, \varphi, z)$ to a point source at $\underline{r}_\circ = (r_\circ, \varphi_\circ, z_\circ)$ with frequency ω . Consider the simplistic ocean waveguide model with constant sound speed c and finite depth d shown in Fig. 1. Furthermore, let G obey the Sommerfeld radiation condition for $r \to \infty$, homogeneous Dirichlet boundary conditions at the ocean surface, and homogeneous Neumann conditions at the ocean bottom. The fundamental solution to the wave equation is expanded in a finite set of propagating normal-modes $\psi_\alpha(z) = \sqrt{2/d}\sin\kappa_\alpha z$ $(\alpha = 1, \ldots, A(\omega))$, which is an accurate approximation if the signal source is located not too closely to the receiving array:

$$G(\underline{r}, \underline{r}_\circ, \omega) = \sum_{\alpha=1}^{A(\omega)} \psi_\alpha(z)\psi_\alpha(z_\circ)\mathrm{H}_0^{(2)}(k_\alpha R), \qquad (1)$$

where $\mathrm{H}_0^{(2)}$ denotes the Hankel function, $z_\circ, z$ are source and horizontal array depth respectively, R is the *horizontal* distance between source and observation point, $|\underline{r} - \underline{r}_\circ|^2 = R^2 + (z - z_\circ)^2$. The contribution of the continuous eigenvalues of the associated Sturm-Liouville equation is neglected. We bounded the number of modes by $A_{\max}$. This is equivalent to a regularization of the inverse problem. Only modes with low grazing angles are included because both relative sensitivities $S_c(k_\alpha) = (c/k_\alpha)|\partial_c k_\alpha|$ and $S_d(k_\alpha) = (d/k_\alpha)|\partial_d k_\alpha|$ increase with mode-number α. Generally, high-order modes are sensitive to environmental parameters (model mismatch and small-scale fluctuations) in contrast to the stability shown by low-order modes [3]. Similar regularization approaches are presented in [4, 6]. In the following, all unknown non-linear parameters are denoted by $\underline{\vartheta} = (\underline{r}_{\circ 1}, \ldots, \underline{r}_{\circ M}, c, d)'$ where M is the number of sources.

3. DATA MODEL

We use the above propagation model to describe the output of the horizontal array of N hydrophones. The array output is sampled after low-pass filtering and sectioned into K stretches of duration T. Each of these data stretches, in turn, is divided into K' time batches of length $T' = T/K'$. Then, they are short-time Fourier-transformed using a multi-window technique to obtain $\underline{X}_{k,\ell}(\omega)$ for $k = 0 \dots K'-1$ and $\ell = 0, \dots, L'-1$. The number L' of orthonormal windows used depends on the selected analysis bandwidth $2W$. Then, the data model reads

$$\underline{X}_{k,\ell}(\omega) = \frac{\mathrm{e}^{-j\omega kT'}}{\sqrt{T'}} \sum_{t=0}^{T'-1} \nu_t^{(\ell)}(T', W)\underline{x}(t+kT')e^{-j\omega t},$$

with a set of orthonormal data tapers $\nu_t^{(\ell)}(T', W)$, the so-called Discrete Prolate Slepian Sequences (DPSS).

The sample estimate of the Cross Spectral Density Matrix (CSDM) $\mathbf{C}_{\underline{x}}(\omega)$ is exploited

$$\hat{\mathbf{C}}_{\underline{x}}(\omega) = \frac{1}{K'L'} \sum_{\ell=0}^{L'-1} \sum_{k=0}^{K'-1} \underline{X}_{k,\ell}(\omega)\underline{X}_{k,\ell}^*(\omega) \qquad (2)$$

during each time step[1]. This is motivated by the asymptotic independence of Fourier-transformed stretches and the orthogonality of the Slepian windows.

Given the signal, the structure of the conditional distribution of $\underline{X}_{k,\ell}(\omega)$ is known asymptotically. The (conditional) covariance matrix is assumed to be $\nu(\omega)\mathbf{I}$, where $\mathbf{I}$ is the identity matrix.

4. MATCHED FIELD CMLE

The asymptotic statistics of the data in frequency domain motivate the application of a CMLE for simultaneous estimation of signal, noise, and environmental parameters. In the broadband case, we can maximize the approximate log-likelihood function $L = L(\underline{\vartheta}, \underline{\nu})$, cf. [7]

$$L = -\frac{1}{J}\sum_{j=1}^{J}\left[N\log\nu(\omega_j) + \frac{\mathrm{tr}(\mathbf{P}^{\perp}(\omega_j, \underline{\vartheta})\hat{\mathbf{C}}_{\underline{x}}(\omega_j))}{\nu(\omega_j)}\right] \qquad (3)$$

where $\underline{\nu} = (\nu(\omega_1)\dots\nu(\omega_J))'$ is the vector of noise spectral parameters and $\underline{\vartheta}$ is defined in Sec. 2. A set of relevant frequencies $\{\omega_1 \dots \omega_J\}$ is selected for maximizing the SNR. $\mathbf{P}^{\perp}(\omega, \underline{\vartheta}) = \mathbf{I} - \mathbf{Q}(\omega, \underline{\vartheta})\mathbf{Q}^*(\omega, \underline{\vartheta})$ is the projection matrix for the noise subspace, where $\mathbf{Q}(\omega, \underline{\vartheta}) = (\underline{q}_1, \dots, \underline{q}_M)$ denotes a matrix whose columns $\underline{q}_m$ form an orthogonal base of the signal space, e.g. $\mathbf{Q}(\omega, \underline{\vartheta}) = \mathbf{H}(\omega; \underline{\vartheta})(\mathbf{H}^*(\omega; \underline{\vartheta})\mathbf{H}(\omega; \underline{\vartheta}))^{-1/2}$. Information about the assumed signal propagation model (i.e. the environmental parameters, which are contained in the Green's function) enters by means of projection matrices, operating on the estimated CSDM. Maximizing (3) over $\underline{\nu}$ leads to the ML estimate $\hat{\nu}(\omega) = \frac{1}{N}\mathrm{tr}\left(\mathbf{P}^{\perp}(\omega, \underline{\vartheta})\hat{\mathbf{C}}_{\underline{x}}(\omega)\right)$.

[1] where $(\cdot)^*$ is the Hermitian transpose.

Re-inserting this into (3) yields the reduced log-likelihood function $l(\underline{\vartheta}) = L(\underline{\vartheta}, \hat{\underline{\nu}})$ which depends on $\underline{\vartheta}$ only

$$l(\underline{\vartheta}) = -\frac{1}{J}\sum_{j=1}^{J}\log(1 - B(\underline{\vartheta}, \omega_j)) + \text{const}\ , \qquad (4)$$

with $B(\underline{\vartheta}, \omega) = \sum_{m=1}^{M} \underline{q}_m^*(\underline{\vartheta}, \omega)\hat{\mathbf{C}}_{\underline{x}}(\omega)\underline{q}_m(\underline{\vartheta}, \omega)/\,\mathrm{tr}\,\hat{\mathbf{C}}_{\underline{x}}(\omega)$. Optimization of $l(\underline{\vartheta})$ is implemented by a combined approach of the globally convergent Genetic Algorithm (GA) and locally convergent Broyden-Fletcher-Goldfarb-Shanno (BFGS) updates for the source positions and ocean depth, where 7 generations of the GA are alternated by one BFGS update.

5. SONAR DATA DESCRIPTION

The experimental site was located in the Bornholm Deep, east of Bornholm island (Baltic Sea). The bathymetry is depicted in Fig. 2. Sonar experiments were conducted by Atlas Elektronik (Bremen) during the cruise between October 3rd and 13th, 1983.

A 15-element hydrophone array with element-spacing 2.56 m was towed by the surface ship *Walther von Ledebur*. A moving broadband source was given by the co-operating ship *Hans Bürkner*. Sound waves originating from two other ships can be detected. Thus the number of broadband sources is set to $M = 4$ (including the towing ship).

Sampling frequency was $f_s = 1024$ Hz after low-pass filtering with cut-off $f_c = 256$ Hz. We use a record of 10 minutes duration, divided into $K = 150$ stretches of $T = 4$ s $= 4096$ samples each. In (2), we averaged over $K' = 16$ Fourier-transformed snapshots of length $T' = 0.25$ s (corresponds to 256 samples). Analysis bandwidth was $2W = 8$ Hz, resulting in $L' = 4$ DPSS data tapers.

STD measurements (salinity, temperature, depth) at the experimental site on 21st September 1983 were provided by ICES (International Council for the Exploration of the Sea, located in Copenhagen). They are acquired from the stationary HELCOM BMP K2 base in the Bornholm Deep at 55° 15′ N 15° 59′ E, see Figs. 2 and 3.

Using formulas from [3], the sound speed profile (SSP) was calculated, see Fig. 3. The SSP shows a sound channel with axis at $z = -50$ m and minimum 1445 m/s.

6. RESULTS

We started our investigation with simulated data. Fig. 4 shows the likelihood (4) as a function of the ocean depth d. The artificial data were generated for a selected ocean depth $d_\circ = 64$ m and $M = 4$ sources present. The broadband single-sensor SNR for this plot is 1.7 dB. In Fig. 4, we plot the conditional likelihood function for the real sonar data versus depth for fixed source coordinates. These two plots show the same qualitative behaviour.

For the real data, we estimated the unknown positions (ranges,bearings, and depths) of $M = 4$ sources and ocean depth assuming the sound speed known and equal to $c = 1500$ m/s. The histogram of source coordinates r, ϕ, z for the final population of the GA is plotted in Fig. 6. The vertical lines indicate the optimum solution. The left-most

vertical lines in the three figures represent the estimates for the *Walther von Ledebur* at endfire position $\phi = 0$.

The ML-estimates for ocean depth are shown in Fig. 5 vs. time. Each time step represents 4s. The individual estimates are mutually independent. Comparing this to the sound speed profile from Fig. 3, we conclude that we actually estimated the onset at $z = -50$ m of increasing sound speed velocity below the sound speed minimum of 1445 m/s.

The median of the estimates in Fig. 5 is 56 m. Remarkable periods of stability in the estimates are observed between time steps 15 and 22, and a systematic trend between time steps 44 and 60 which possibly stems from the movement of the towed array. The repeated outliers at approximately 70 m and 47 m result from the ambiguity of the likelihood function. The simulations below have much lower spread than the real data. This indicates model mismatch, as is expected from the over-simplistic assumptions in Section 2.

The scenario in Fig. 1 was selected to compute the accuracy of estimating the parameters of interest with a single source at $r_\circ = 2000$ m, $\phi_\circ = 45°$, $z_\circ = -5$ m using the nominal value $d = 56$ m. The temporally white signal and noise were assumed to occupy the full bandwidth $0 \ldots 256$ Hz with SNR $= 3$ dB.

Fig. 7 shows the scatterplots of estimates from Monte Carlo (MC) simulations. From the results in Fig. 7, it is directly observed that the estimates for source location $\hat{r}_\circ, \hat{\phi}_\circ, \hat{z}_\circ$ have low mutual correlation, as is expected from CRB in a known waveguide [8]. Also, both source bearing $\hat{\phi}_\circ$ and depth $\hat{z}_\circ$ have low correlation with environmental parameters.

Environmental estimates $\hat{c}$ and $\hat{d}$ turn-out to be highly correlated. The mutual correlation results in a simple rescaling by a factor λ of the ocean waveguide with parameters (c, d). In this way, the cut-off frequencies $f_\alpha = (2\alpha+1)c/4d$, $(\alpha = 0, 1, \ldots)$ are invariant for the re-scaled waveguide with $(\lambda c, \lambda d)$. Thereby, the dispersion diagram is qualitatively unchanged and only the wavenumbers are rescaled: $k_\alpha \rightarrow \lambda^{-1} k_\alpha$. This scaling only applies to the waveguide. The hydrophone array is not changed – otherwise, this would result in an identification problem. Due to a slight sound speed mismatch for the real data (assumed 1500 m/s vs. 1445–1480 m/s, cf. Fig. 3) and this type of mutual correlation, we expect a 2–3% bias in the ocean depth estimate.

The final marginal distributions of the estimates are shown in Fig. 8. These histograms are based on the same data as in Fig. 7. We observe good concentration of the estimates for source range, bearing, sound speed, and ocean depth. Source depth, however, shows considerably more spread.

7. CONCLUSION

Experimental results are presented on estimating an environmental parameter (ocean depth) using several unknown broadband acoustic sources. The obtained results imply feasibility of *purely passive* bathymetry for low SNR which can be extended to geo-acoustic inversion.

8. REFERENCES

[1] *Proc. of Full-field inversion methods in ocean and seismo-acoustics*, O. Diachok, A. Caiti, P. Gerstoft, and H. Schmidt, Eds., 1995, Kluwer.

[2] S.M. Jesus, A. Caiti, and H. Zambujo, "Geophysical seafloor monitoring with a towed array in shallow water, 12-month progress report", Tech. Rep. MAS2-CT920022, Economic European Community, 1993.

[3] F.B. Jensen, W.A. Kuperman, M.B. Porter, and H. Schmidt, *Computational Ocean Acoustics*, American Institute of Physics Press, New York, 1994.

[4] J. Tabrikian, J. Krolik, and H. Messer, "Robust maximum likelihood localization by exploiting predictable acoustic modes", in *Proc. ICASSP*, Atlanta, 1996.

[5] A. Caiti and S.M. Jesus, "Acoustic estimation of seafloor parameters: a radial basis functions approach", *J. Acoust. Soc. Am.*, Sept. 1996.

[6] A.B. Baggeroer and E.K. Scheer, "Stochastic matched field processing", 138^{th} ASA Meeting, 1pUW2, Columbus, Ohio, Nov. 1999.

[7] J.F. Böhme, "Array processing", in *Advances in Spectrum Analysis and Array Processing*, S. Haykin, Ed., pp. 1–63. Prentice-Hall, Englewood Cliffs, 1991.

[8] *Acoustic Signal Processing for Ocean Exploration*, J.M.F. Moura and I.M.G. Lourtie, Eds., Reidel, 1992.

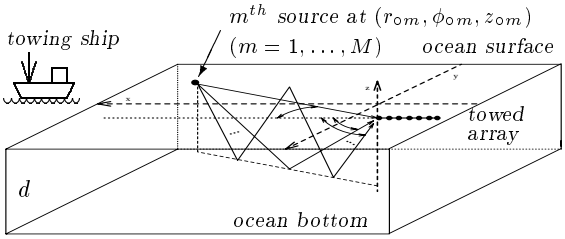

Figure 1: One-layer ocean model with sound speed c and ocean depth d.

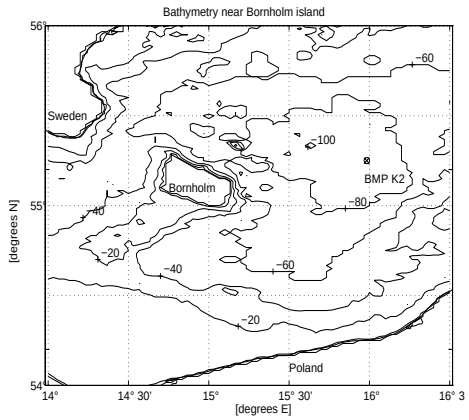

Figure 2: High-resolution bathymetry at experimental site in Baltic Sea.

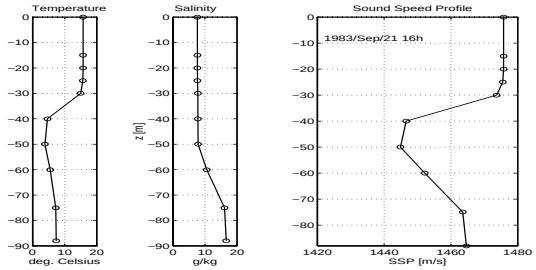

Figure 3: STD profiles on Sept. 21, 1983, 16:00 (local time). SSP is calculated from salinity and temperature.

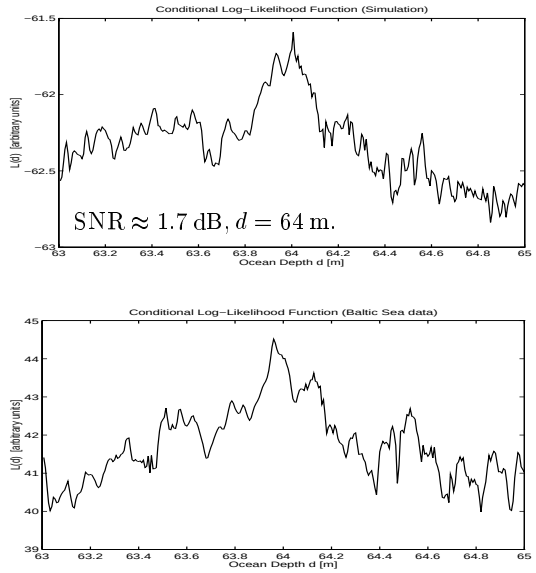

Figure 4: Typical $l(\underline{\vartheta})$-function, Eq.(4), vs. ocean depth. Top: simulated, Bottom: real data.

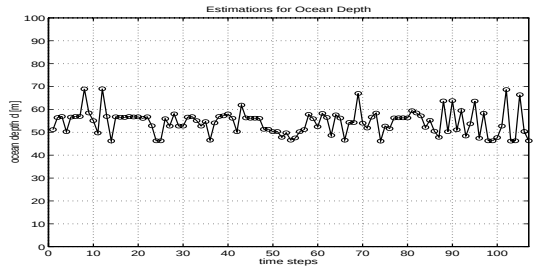

Figure 5: estimates for ocean depth $\hat{d}$ for snapshots of 4s duration.

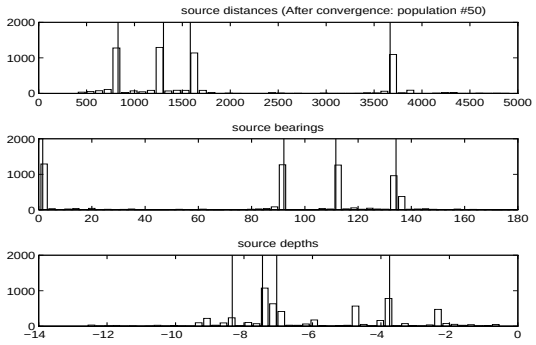

Figure 6: Posteriori distribution of genetic algorithm: 12 estimated source coordinates ($M = 4$ sources) and ocean depth.

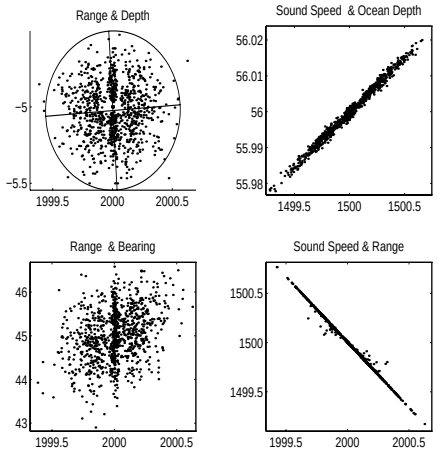

Figure 7: Scatterplot of 1000 MC Simulations.

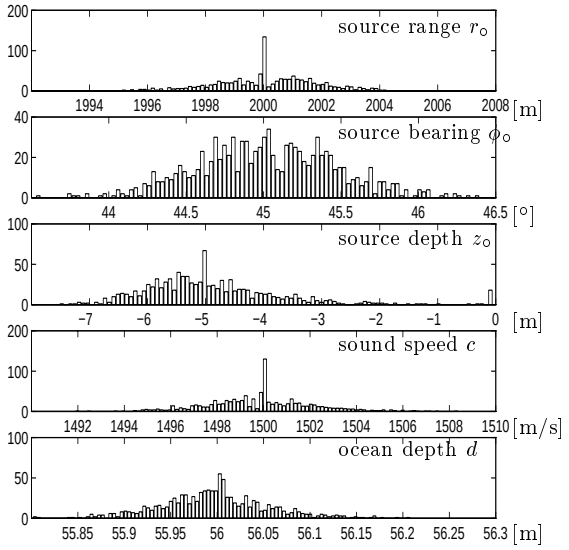

Figure 8: Parameter histograms for MC simulation result.